Progress In Electromagnetics Research C, Vol. 172, 135–145, 2026

(Received 3 June 2026, Accepted 2 July 2026, Scheduled 3 August 2026)

Optimal Configuration of AC Filters in Hybrid Multi-Infeed HVDC Systems Based on Sensitivity Analysis

Wenxing Sun[1], Lihua Liu[2], Weixi He[2,*], Xueliang Liu[1], Jiawen Lai[1], and Junju Lai[1]

[1]*Qingyuan Power Supply Bureau of Guangdong Power Grid Co., Ltd., Qingyuan, Guangdong 511500, China*
[2]*North China Electric Power University, Baoding 071003, China*

ABSTRACT: To address the challenges of coordinating local reactive power compensation with cross-station harmonic interaction suppression in hybrid multi-infeed HVDC (HMIDC) systems, this study proposes an optimal AC filter configuration method based on sensitivity analysis. A harmonic impedance equivalent model was established for a hybrid three-infeed HVDC system, and a comprehensive harmonic interaction index was constructed based on harmonic current interaction influence coefficients. Normalized sensitivity analysis was then performed on the AC filter impedance, receiving-end AC system impedance, and tie-line impedance at the 11th and 13th harmonics. The results indicate that the AC filter impedance serves as the dominant adjustable factor. On this basis, a discrete optimization model was developed, with the number of DT11/24 and DT13/36 double-tuned filter groups in service as decision variables. In addition, this model considers equipment limits, minimum filtering requirements, reactive power compensation, and harmonic voltage constraints. Case study results show that the optimized configuration reduces the overall harmonic coupling among HVDC infeed systems; in particular, the interaction strength from the second conventional HVDC link to the modular multilevel converter-based high-voltage direct current (MMC-HVDC) link at the 13th harmonic decreases by approximately 32%. The proposed method provides a practical reference for coordinated AC filter switching in HMIDC.

1. INTRODUCTION

With the continuous development of line-commutated converter-based high-voltage direct current (LCC-HVDC) projects and modular multilevel converter-based high-voltage direct current (MMC-HVDC) projects, the operating pattern, where multiple HVDC transmission systems are concentrated in the same receiving-end AC grid, has become increasingly prominent. In particular, after the commissioning of projects such as the Wudongde UHV multi-terminal DC project and Baihetan-Jiangsu UHV hybrid cascaded DC project, LCC-HVDC and MMC-HVDC systems have coexisted in receiving-end power grids, gradually forming hybrid multi-infeed HVDC (HMIDC) systems [1, 2]. LCC-HVDC has the advantages of large transmission capacity and mature technology; however, its commutation process inevitably generates characteristic harmonics, such as the 11th and 13th harmonics. Although MMC-HVDC generally produces a lower harmonic content on the AC side, its AC-side impedance still participates in the system's harmonic network. When LCC-HVDC and MMC-HVDC systems are connected to the same receiving-end AC grid, electrical coupling occurs among different converter stations through the AC network. Harmonic currents generated by one converter station may propagate to other converter stations via AC tie lines, causing cross-station harmonic interaction, harmonic amplification, and resonance. Therefore, investigating the harmonic interaction characteristics of HMIDC systems and their suppression methods is of great significance for improving power quality and ensuring the stable operation of receiving-end AC grids.

Extensive studies have been conducted on the harmonic impedance modeling of HVDC systems and the interaction effects in multi-infeed HVDC systems. Studies on LCC-HVDC have investigated harmonic generation mechanisms, harmonic transfer characteristics, and impedance modeling methods, providing a theoretical basis for analyzing the harmonic response of conventional HVDC converter stations across different frequencies [3–7]. The harmonic characteristics of HVDC systems have also been analyzed from the perspectives of harmonic impedance scanning, equivalent harmonic impedance calculation, and harmonic transfer between the AC and DC sides [8–10]. Existing studies on MMC-HVDC systems have developed AC-side impedance models and revealed frequency coupling among arm currents, submodule capacitor voltages, and control loops. The results indicate that the AC-side impedance of the MMC affects harmonic response characteristics of the overall system [11–13]. Further research has focused on the interaction mechanisms in multi-infeed and hybrid multi-infeed HVDC systems, proposing evaluation methods such as multi-infeed interaction factors and harmonic impedance matrices, which provide a basis for quantitatively assessing the harmonic interaction strength among different HVDC infeed systems [14–19]. In addition, the AC filter's optimization design was conducted to enhance the operating performance of HVDC transmission systems [20].

The aforementioned studies provide a significant foundation for harmonic interaction modeling, interaction index construc-

* Corresponding author: Weixi He (2284518036@qq.com).

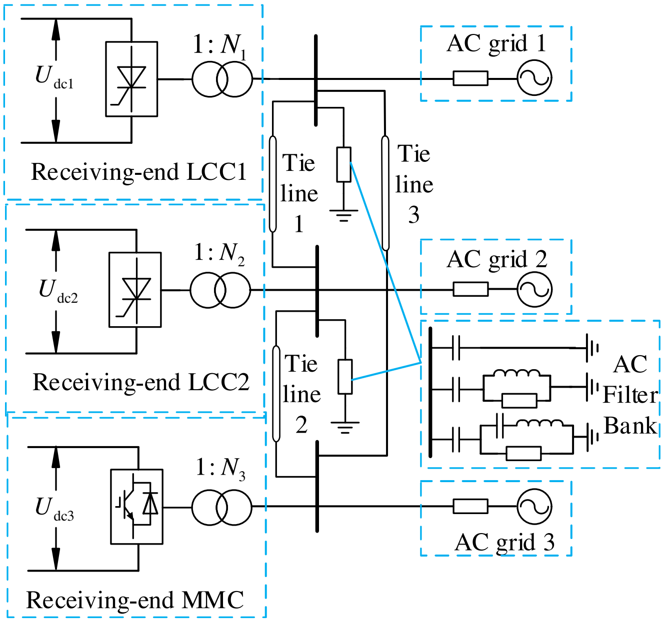

FIGURE 1. Model of the hybrid three-infeed HVDC transmission system.

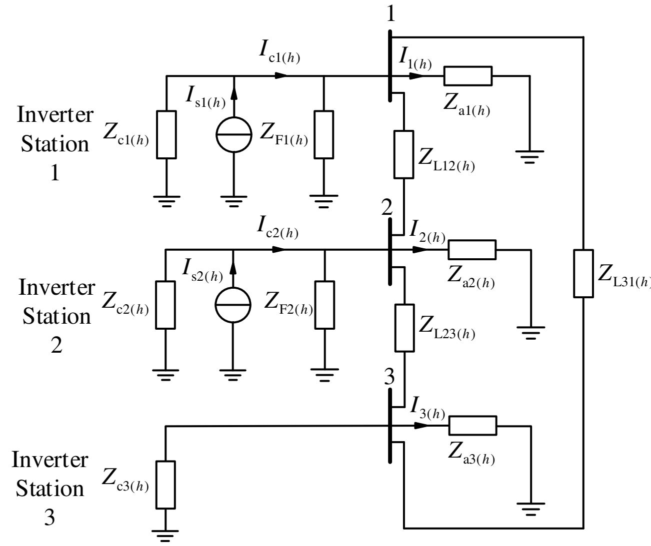

FIGURE 2. Harmonic interaction impedance analysis model of the hybrid three-infeed system.

tion, and AC filter design in HMIDC systems. However, several limitations remain. On the one hand, existing research mainly focuses on converter station impedance modeling or harmonic interaction mechanisms; conversely, insufficient attention has been paid to the system-level variation of harmonic interactions induced by changes in AC filter parameters and switching states. On the other hand, traditional methods for AC filter configuration are usually based on local harmonic suppression, reactive power compensation, and power quality constraints of a single converter station, with limited consideration of how filter switching affects harmonic current distribution and cross-station interaction strength in other infeed DC systems from the perspective of the entire HMIDC system. Therefore, it is necessary to develop an optimal configuration method for AC filters, oriented toward the suppression of overall system harmonic interactions.

Accordingly, this study proposes an optimal AC filter configuration method for HMIDC systems based on sensitivity analysis. First, a harmonic impedance analysis model of the hybrid multi-infeed HVDC system was established, and a comprehensive harmonic interaction index was constructed based on the harmonic current interaction influence coefficients. Second, a normalized sensitivity index is defined, and comprehensive sensitivity analysis is performed on AC filter parameters, receiving-end AC system impedance parameters, and tie-line impedance parameters to identify the key factors affecting harmonic interactions. Third, under typical operating conditions, the impact of the AC filter switching states on the harmonic interactions among different HVDC infeed systems was analyzed. Finally, taking the discrete numbers of double-tuned filter groups in service at two conventional HVDC converter stations as decision variables, an AC filter optimal configuration model is established considering equipment configuration, minimum filtering requirements, reactive power balance, and power quality constraints. The model was solved using a discrete particle swarm optimization algorithm, and the results validated the effectiveness of the proposed method in reducing harmonic interactions within HMIDC systems.

2. HARMONIC INTERACTION INFLUENCE COEFFICIENTS IN HYBRID MULTI-INFEED HVDC SYSTEMS

2.1. Harmonic Impedance Equivalent Model of the Hybrid Multi-Infeed DC System

A hybrid three-infeed HVDC system in which two conventional HVDC links and one flexible HVDC link are jointly fed into the receiving-end AC network is selected as the study object, as shown in Fig. 1.

From the perspective of the AC-side port, an LCC-HVDC converter station generates characteristic harmonics, such as the 11th and 13th harmonics, during operation. Therefore, it can be equivalently represented as a harmonic current source connected in parallel with an AC-side equivalent harmonic impedance. Since the quality of the AC-side output waveform of MMC-HVDC is high and the harmonic current injected into the AC system is relatively small, only the effect of its AC-side equivalent harmonic impedance on the system harmonic current distribution is considered. The simplified model is shown in Fig. 2.

In Fig. 2, $Z_{cn(h)}$ denotes the AC-side equivalent harmonic impedance of the inverter station of the n-th DC link at the h-th harmonic; $Z_{Fn(h)}$ denotes the equivalent harmonic impedance of the AC filters and reactive power compensation devices on the inverter-station side of the n-th DC link; $Z_{L12(h)}$, $Z_{L23(h)}$, and $Z_{L31(h)}$ denote the equivalent harmonic impedances of the tie lines among different DC links; and $Z_{an(h)}$ denotes the equivalent harmonic impedance of the receiving-end AC system into which the n-th DC link is fed. The equivalent harmonic current sources of the two LCC-HVDC links at the h-th harmonic are denoted as $I_{s1(h)}$ and $I_{s2(h)}$, respectively, and the harmonic currents flowing from the infeed nodes into the AC system are denoted as $I_{1(h)}$, $I_{2(h)}$, and $I_{3(h)}$, respectively.

According to this model, when the harmonic current generated by one conventional DC link changes, it affects the harmonic content at other nodes via tie lines, thereby inducing harmonic interactions. To facilitate subsequent quantitative analysis, a harmonic current interaction influence coefficient is introduced to characterize the harmonic interaction strength among different DC links in an HMIDC system.

2.2. Harmonic Current Interaction Influence Coefficients

The harmonic current interaction influence coefficient is defined as follows:

$$\alpha_{ij(h)} = \dot{I}_{i(h)}/\dot{I}_{sj(h)} \tag{1}$$

This coefficient represents the current response at the target node after the harmonic source current is distributed through the system impedance network. A larger magnitude indicates a stronger harmonic influence of the j-th conventional DC link on the i-th node.

According to the harmonic impedance equivalent model shown in Fig. 2, the relationship between the AC-side equivalent harmonic current sources of the converter stations and the harmonic currents flowing from each node into the AC system can be expressed as follows:

$$\begin{bmatrix} \dot{I}_{1(h)} \\ \dot{I}_{2(h)} \\ \dot{I}_{3(h)} \end{bmatrix} = \begin{bmatrix} \alpha_{11(h)} & \alpha_{12(h)} \\ \alpha_{21(h)} & \alpha_{22(h)} \\ \alpha_{31(h)} & \alpha_{32(h)} \end{bmatrix} \begin{bmatrix} \dot{I}_{(s1(h))} \\ \dot{I}_{s(s2(h))} \end{bmatrix} \tag{2}$$

Based on Equation (2), the harmonic current interaction influence coefficients among different DC links can be further derived. For the harmonic interaction between the two LCC-HVDC links, the interaction influence coefficients are expressed as follows:

$$\alpha_{12(h)} = \frac{\dfrac{1}{Z_{\text{L12}(h)}} Z_{3(h)} + \dfrac{1}{Z_{\text{L23}(h)}} Z_{\text{L31}(h)}}{Z_{\text{a1}(h)} Z_{\Delta(h)}} \tag{3}$$

$$\alpha_{21(h)} = \frac{\dfrac{1}{Z_{\text{L12}(h)}} Z_{3(h)} + \dfrac{1}{Z_{\text{L23}(h)}} Z_{\text{L31}(h)}}{Z_{\text{a2}(h)} Z_{\Delta(h)}} \tag{4}$$

where,

$$Z_{1(h)} = \frac{1}{Z_{c1(h)}} + \frac{1}{Z_{F1(h)}} + \frac{1}{Z_{a1(h)}} + \frac{1}{Z_{L12(h)}} + \frac{1}{Z_{L31(h)}} \tag{5}$$

$$Z_{2(h)} = \frac{1}{Z_{c2(h)}} + \frac{1}{Z_{F2(h)}} + \frac{1}{Z_{a2(h)}} + \frac{1}{Z_{L12(h)}} + \frac{1}{Z_{L23(h)}} \tag{6}$$

$$Z_{3(h)} = \frac{1}{Z_{c3(h)}} + \frac{1}{Z_{a3(h)}} + \frac{1}{Z_{L23(h)}} + \frac{1}{Z_{L31(h)}} \tag{7}$$

$$Z_{\Delta(h)} = Z_{1(h)} Z_{2(h)} Z_{3(h)} - \frac{Z_{1(h)}}{Z^2_{\text{L23}(h)}} - \frac{Z_{2(h)}}{Z^2_{\text{L31}(h)}} \tag{8}$$

Similarly, the interaction influence coefficients between the LCC-HVDC and MMC-HVDC links are expressed as follows:

$$\alpha_{31(h)} = \frac{\dfrac{1}{Z_{L31(h)}} Z_{2(h)} + \dfrac{1}{Z_{L12(h)}} Z_{L23(h)}}{Z_{a3(h)} Z_{\Delta(h)}} \tag{9}$$

$$\alpha_{32(h)} = \frac{\dfrac{1}{Z_{L23(h)}} Z_{1(h)} + \dfrac{1}{Z_{L12(h)}} Z_{L31(h)}}{Z_{a3(h)} Z_{\Delta(h)}} \tag{10}$$

3. SENSITIVITY ANALYSIS METHOD FOR HARMONIC INTERACTION INFLUENCE

3.1. Definition of the Sensitivity Index

In practical applications, engineering applications primarily focus on the variation trend of the harmonic interaction strength. Consequently, the magnitude of the harmonic current interaction influence coefficient was employed as the analysis object. Considering the harmonic effects of the two conventional DC links at their respective nodes, their mutual interactions, and their harmonic interactions with the MMC-HVDC link, the comprehensive harmonic interaction influence index is defined as follows:

$$|\alpha_\Sigma(h)| = \sum_{i\in\{1,2\}} |\alpha_{ii}(h)| + \sum_{\substack{i,j\in\{1,2\} \\ i\neq j}} |\alpha_{ij}(h)| + \sum_{k\in\{1,2\}} |\alpha_{3k}(h)| \tag{11}$$

where the first term represents the harmonic effect of the two conventional DC links at their respective nodes; the second term represents the harmonic interaction between the two conventional DC links; and the third term represents the harmonic interaction from the two conventional DC links to the MMC-HVDC link.

The comprehensive harmonic interaction influence index therefore comprises three components: the local harmonic effect of each conventional DC link, the harmonic interaction between the two LCC-HVDC links, and the harmonic influence of the LCC-HVDC links on the MMC-HVDC link.

By combining these components, the index characterizes the overall redistribution of harmonic currents among the converter stations through the coupled receiving-end AC network. Since variations in filter impedance may affect the local harmonic responses and the cross-station interaction channels differently, the aggregated index provides a system-level measure of harmonic interaction under a given operating condition.

To compare the effects of parameters with different units and base magnitudes on a common dimensionless basis, the normalized sensitivity index is defined as follows:

$$S_p^\Sigma(h) = \left| \frac{\partial |\alpha_\Sigma(h)| / |\alpha_{\Sigma,0}(h)|}{\partial p / p_0} \right| \approx \left| \frac{\Delta |\alpha_\Sigma(h)|}{\Delta p} \cdot \frac{p_0}{|\alpha_{\Sigma,0}(h)|} \right| \tag{12}$$

where $|\alpha_{\Sigma,0}(h)|$ denotes the comprehensive harmonic interaction index of the HMIDC system at the h-th harmonic under base operating condition; p_0 is the base value of parameter p; $\Delta|\alpha_\Sigma(h)|$ and Δp denote the variations in the comprehensive harmonic interaction index and the corresponding parameter before and after perturbation, respectively. A larger $S_p^\Sigma(h)$ indicates that the variation of this parameter has a more significant influence on the harmonic interaction in the HMIDC system at the corresponding harmonic order; otherwise, its influence is weaker.

3.2. Comprehensive Sensitivity Ranking and Key Parameter Identification

To identify the dominant factors affecting harmonic interactions in the HMIDC system, the equivalent impedances of the receiving-end AC systems, the tie-line impedances between converter stations, and the equivalent impedances of the AC filters at the conventional HVDC converter stations are selected as analysis objects. The normalized sensitivity indices of these parameters at the 11th and 13th characteristic harmonics are calculated and ranked, as shown in Fig. 3.

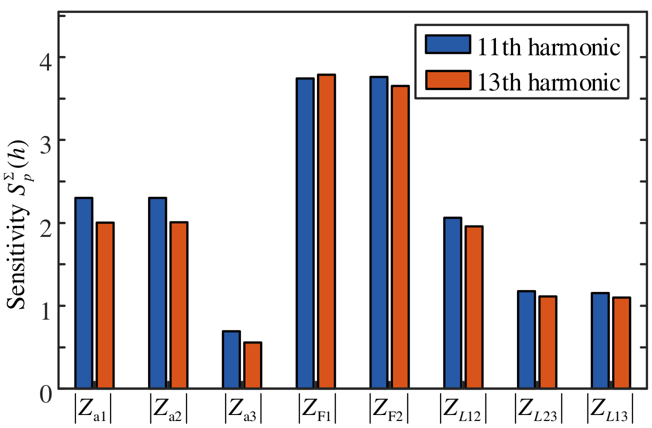

FIGURE 3. Sensitivity ranking.

In Fig. 3, Z_{a1}, Z_{a2}, and Z_{a3} denote the equivalent impedance parameters of the receiving-end AC systems connected to the three DC links; Z_{L12}, Z_{L23}, and Z_{L13} denote the tie-line parameters among different converter stations; Z_{F1} and Z_{F2} denote the AC filter parameters at the two conventional HVDC converter stations.

At the 11th and 13th characteristic harmonics, the sensitivities associated with the AC filter parameters are generally higher than those associated with the receiving-end AC system and tie-line impedances, as shown in Fig. 3. The double-tuned filters operate near their low-impedance regions at these characteristic frequencies; therefore, variations in filter impedance directly modify the local harmonic shunt paths and the nodal current distribution in the coupled AC network. Moreover, the filter-bank operating states can be adjusted during system operation, whereas the receiving-end system and tie-line impedances are primarily determined by the existing network structure. The AC filter switching states are therefore selected as the decision variables for the subsequent optimal configuration.

4. INFLUENCE OF AC FILTER SWITCHING ON HARMONIC INTERACTIONS

4.1. AC Filter Configuration Scheme

On the AC side of conventional HVDC converter stations, multiple filter groups and reactive power compensation devices are typically configured to satisfy the requirements of characteristic harmonic suppression and reactive power compensation simultaneously. The filter equipment considered in this study mainly includes DT11/24 double-tuned filters, DT13/36 double-tuned filters, HP3 high-pass filters, and SC shunt capacitors. In practical engineering, multiple filter groups are typically connected in parallel. The structures and parameters of the filters and shunt capacitors are listed in Table 1, and their wiring diagrams are shown in Fig. 4.

TABLE 1. AC filter parameters.

Component parameter	Filter group type			
	DT11/24	DT13/36	HP3	SC
$C_1/\mu\text{F}$	2.32	2.30	2.31	2.159
L_1/mH	12.52	6.01	641.33	2.039
$C_2/\mu\text{F}$	5.46	3.90	15.80	–
L_2/mH	9.33	8.73	–	–

The parameters listed in Table 1 were obtained from the engineering design data provided by the equipment manufacturer for the studied converter stations. In practical converter stations, each AC filter bank mainly comprises high-voltage capacitor units, tuning reactors, damping resistors, together with the associated switching and protection equipment and bus connections. In the harmonic interaction model, the main filtering components are represented by the lumped-parameter equivalent circuits shown in Fig. 4.

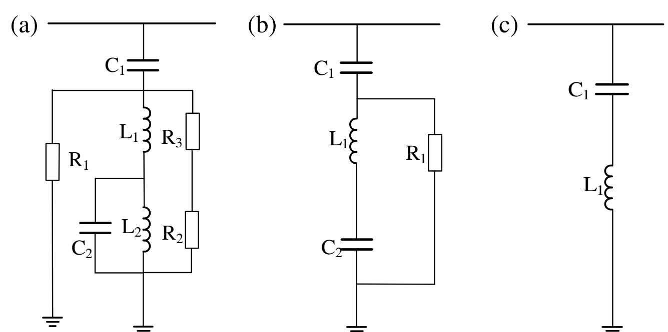

FIGURE 4. Wiring diagrams of AC filters and shunt capacitors. (a) Double-tuned filter, (b) HP3 filter, and (c) SC capacitor.

The tuning reactors are dry-type air-core reactors and therefore do not involve magnetic-core saturation or core losses. The equivalent series resistance of the capacitors and the winding resistance of the reactors determine the damping and quality factor of the tuned branches, thereby affecting the min-

TABLE 2. AC filter switching strategies under different DC power conditions.

Operating mode	DC power/MW	SC	DT11/24	DT13/36
Bipolar full-voltage operation	5000	6	4	4
80% reduced-voltage operation	4000	3	4	4
50% reduced-voltage operation	2500	0	4	4
30% reduced-voltage operation	1500	0	3	2

imum impedance and bandwidth around the tuning frequencies [21]. The equivalent series inductance of the capacitors and the parasitic capacitance of the reactors mainly influence the high-frequency and self-resonant characteristics of the components [22]. Since the present analysis focuses on the steady-state 11th- and 13th-order harmonics, the principal tuning characteristics are represented using the nominal inductance and capacitance parameters.

Impedance-frequency characteristics of the AC filters are shown in Fig. 5. For a fundamental frequency of 50 Hz, the DT11/24 filter exhibits two low-impedance valleys near 550 Hz and 1200 Hz, corresponding to the 11th- and 24th-order harmonics, respectively. The DT13/36 filter similarly exhibits low-impedance valleys near 650 Hz and 1800 Hz, corresponding to the 13th- and 36th-order harmonics. Therefore, the corresponding characteristic harmonic currents can be preferentially diverted into the filter branches rather than injected into the receiving-end AC network. Impedance peaks can also be observed between the two tuning frequencies of each double-tuned filter, which result from inherent anti-resonance characteristics of the double-tuned circuits. In comparison, the HP3 filter reaches its minimum impedance near 150 Hz, corresponding to the third-order harmonic, and its impedance subsequently increases smoothly toward a finite value because of the damping resistor. This characteristic provides broadband harmonic damping rather than selective filtering at only a few discrete harmonic frequencies.

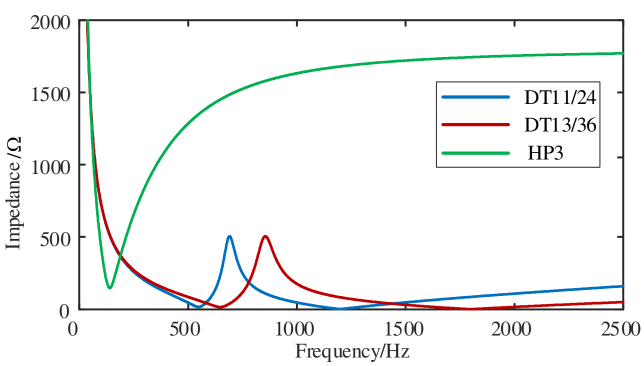

FIGURE 5. Frequency-impedance curves of the filters.

According to the actual engineering configuration, the receiving-end converter station of the first conventional DC link is equipped with four DT11/24 filter groups, four DT13/36 filter groups, and six SC shunt capacitor groups. The capacity of each double-tuned filter group was 197 Mvar, and the capacity of each SC shunt capacitor group was 238 Mvar. The receiving-end converter station of the second conventional DC link is equipped with four DT11/24 filter groups, three DT13/36 filter groups, and seven SC shunt capacitor groups. The capacity of each double-tuned filter group was 195 Mvar, and the capacity of each SC shunt capacitor group was 235 Mvar.

To further illustrate the filtering effect of the above AC filter models, time-domain simulations were performed using the engineering design parameters listed in Table 1. The converter operating condition, harmonic-source parameters, receiving-end AC system impedance, and tie-line parameters were kept unchanged, with only the AC filter connection state varied. Fig. 6 compares the current I_1 flowing from the first LCC-HVDC infeed node into the receiving-end AC system, together with its harmonic current ratios, for cases with and without the AC filters.

As shown in Fig. 6, without AC filters, the current waveform exhibits evident distortion, and relatively large harmonic components appear at 550 Hz and 650 Hz, corresponding to the 11th- and 13th-order characteristic harmonics, respectively. After the AC filters are connected, the current waveform becomes smoother, and both harmonic current ratios decrease markedly. These results agree with the low-impedance characteristics of DT11/24 and DT13/36 filters shown in Fig. 6 and demonstrate the expected suppression of the corresponding characteristic harmonics.

4.2. AC Filter Switching Strategies under Typical Operating Conditions

Conventional HVDC transmission systems typically employ reactive power control (RPC) for the discrete group switching of AC filters and shunt capacitors. The control structure is shown in Fig. 7.

Based on the RPC hierarchical control logic and the actual AC filter configurations of the two conventional HVDC converter stations, the number of SC shunt capacitor groups in service first decreases as DC transmission power decreases. When the system operates at a reduced power level, the number of double-tuned filter groups is adjusted accordingly. The filter switching strategies under different DC power conditions are presented in Table 2.

4.3. Influence of AC Filter Switching States on Harmonic Interactions

To quantitatively analyze the influence of double-tuned filter switching on harmonic interaction strength, the first conventional DC link is initially assumed to operate at 50% rated power with eight double-tuned filter groups in service, and the

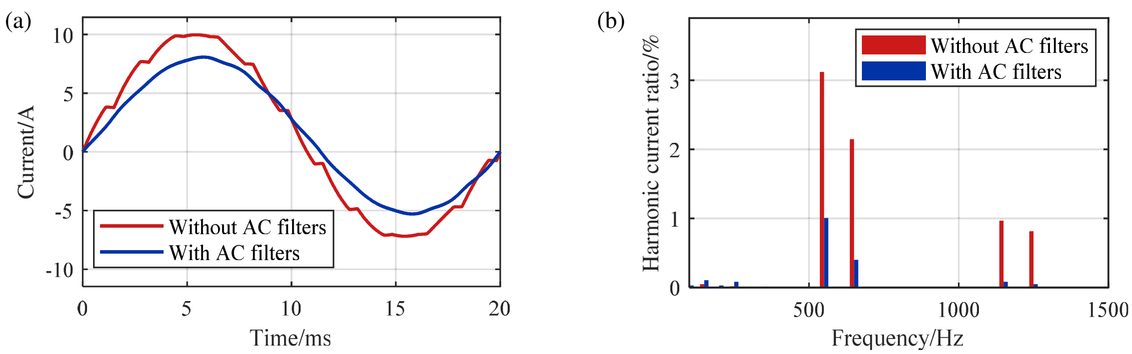

FIGURE 6. Comparison of AC-side current waveforms and harmonic current ratios with and without AC filters. (a) Current waveforms and (b) harmonic current ratios.

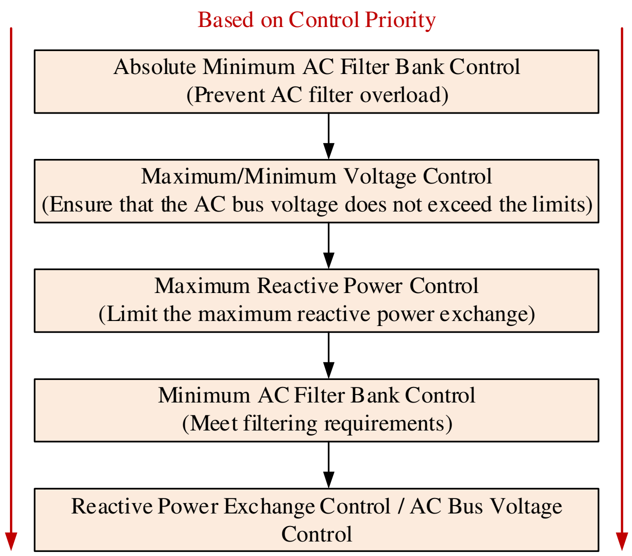

FIGURE 7. Conventional reactive power control structure.

second conventional DC link operates at 45% rated power with seven double-tuned filter groups in service. When the operating power of the first conventional DC link decreases to 30% of the rated power, certain AC filters must be switched out to prevent excessive reactive power and meet operating constraints. As a typical switching scenario, one DT11/24 filter group and two DT13/36 filter groups were switched out. The magnitudes of the harmonic current interaction influence coefficients before and after switching at the 11th and 13th harmonics were calculated, and the results are presented in Fig. 8.

As shown in Fig. 8, after the AC filters of the first conventional DC link are disconnected, the harmonic current flowing from this link into the AC system increases, and the harmonic currents in the other two links also increase. This indicates that the AC filter switching state changes the harmonic interaction relationships among the different DC links within the system.

A reduction in filter impedance strengthens the local harmonic shunt path and limits the propagation of the corresponding harmonic current through the common AC network, whereas filter removal increases the branch impedance and redistributes a larger proportion of the harmonic current toward the interconnected nodes.

Further analysis shows that the harmonic current interaction influence coefficients are related not only to the filter groups in service in a single link but also to the combination of double-tuned filter group numbers in the two conventional DC links. When the number of double-tuned filter groups in service decreases, the corresponding harmonic interaction influence coefficients generally increase. Therefore, the AC filter configuration should be coordinated from the overall system perspective rather than determined solely by the local reactive power demand or harmonic mitigation requirement of a single converter station. This observation motivated the establishment of an optimal AC filter configuration model aimed at reducing the overall harmonic interaction level of the HMIDC system.

5. AC FILTER OPTIMAL CONFIGURATION MODEL BASED ON THE DISCRETE PARTICLE SWARM OPTIMIZATION ALGORITHM

5.1. Constraints

To ensure that the optimization results align with the requirements of practical engineering operations, the filters' inductance and capacitance parameters were not continuously optimized. Instead, the number of double-tuned filter groups in service is directly selected as a decision variable:

$$\mathbf{X} = [n_{\mathrm{DT11},1},\ n_{\mathrm{DT13},1},\ n_{\mathrm{DT11},2},\ n_{\mathrm{DT13},2}]^{\mathrm{T}} \tag{13}$$

where $n_{\mathrm{DT11},i}$ and $n_{\mathrm{DT13},i}$ denote the actual numbers of DT11/24 and DT13/36 filter groups in service at the i-th converter station, respectively.

To prevent the optimization results from exceeding the practical operating boundaries, the following constraints were imposed.

5.1.1. Equipment Configuration Constraints

The number of filter groups in service cannot exceed the number of devices installed at the converter station. Let $N_{\mathrm{D11},i}^{\max}$ and $N_{\mathrm{D13},i}^{\max}$ denote the maximum numbers of DT11/24 and DT13/36 filter groups that can be put into service in the i-th link, respectively. Then

$$0 \le n_{\mathrm{D11},i} \le N_{\mathrm{D11},i}^{\max}, \quad N_{\mathrm{D11},i} \in Z \tag{14}$$

$$0 \le n_{\mathrm{D13},i} \le N_{\mathrm{D13},i}^{\max}, \quad N_{\mathrm{D13},i} \in Z \tag{15}$$

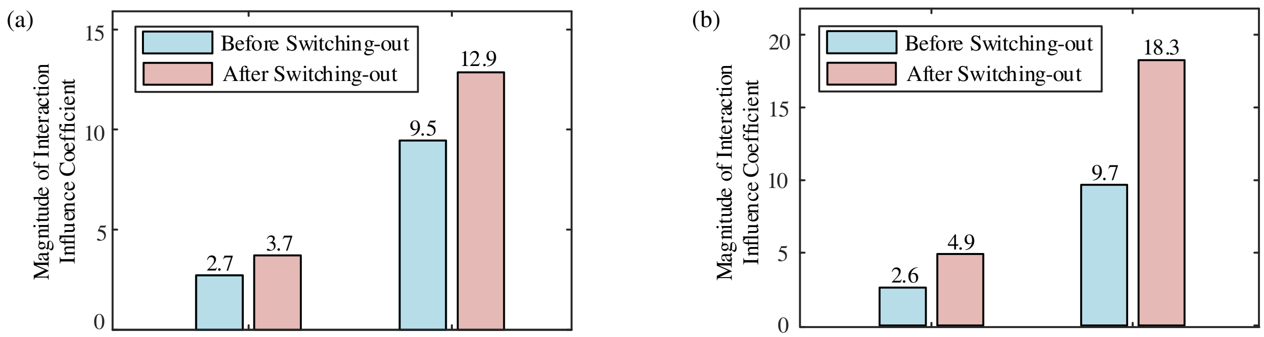

FIGURE 8. Comparison of harmonic current interaction influence coefficient magnitudes before and after switching. (a) 11th harmonic and (b) 13th harmonic.

TABLE 3. Limits for harmonics in public power grids specified in GB/T 14549-1993.

Voltage level/kV	Total harmonic voltage distortion/%	Individual harmonic voltage	
		Odd harmonics	Even harmonics
0.38	5	4	2
6, 10	4	3.2	1.6
35, 66	3	2.4	1.2
110	2	1.6	0.8

where $i = 1, 2$.

5.1.2. Minimum Filtering-Capacity Constraint

Under low-power operation, although the reactive power demand of converter station decreases, the characteristic harmonics generated by the LCC-HVDC system still require suppression by AC filters. Therefore, double-tuned filters should not be switched excessively and must satisfy the minimum filtering requirements. For the i-th link, the minimum filtering constraint is given by:

$$n_{11,i} + n_{13,i} \geq N_i^{\min}, \quad i = 1, 2 \tag{16}$$

where $N_i^{\min}$ is the minimum total number of double-tuned filter groups required by the i-th link to satisfy the basic filtering requirement.

5.1.3. Reactive Power Balance Constraint

In addition to harmonic suppression, double-tuned filters provide reactive power to the AC-bus. Let the reactive power compensation provided by the double-tuned filters in the i-th link under configuration $\mathbf{X}$ be

$$Q_{F,i}(\mathbf{X}) = n_{11,i}Q_{11,i} + n_{13,i}Q_{13,i} \tag{17}$$

where $Q_{11,i}$ and $Q_{13,i}$ denote the reactive power capacities provided by one DT11/24 filter group and one DT13/36 filter group in the i-th link, respectively. The reactive power balance constraint is then expressed as

$$Q_{\min,i} \leq Q_{F,i}(\mathbf{X}) \leq Q_{\max,i}, \quad i = 1, 2 \tag{18}$$

where $Q_{\min,i}$ and $Q_{\max,i}$ denote the lower and upper limits of the reactive power required by the i-th link under the current operating mode, respectively.

5.1.4. Power Quality Constraint

The optimized filter configuration should satisfy the power-quality requirements specified by the national grid operating standards. Therefore, under any filter switching combination, the harmonic ratio of voltage (HRU) for individual harmonics and the total harmonic distortion of voltage (THDU) at the AC buses of all converter stations must not exceed the prescribed limits:

$$\begin{cases} \mathrm{HRU}_{h,i}(\mathbf{X}) = \dfrac{U_{h,i}(\mathbf{X})}{U_{1,i}} \times 100\% \leq \mathrm{HRU}_{\max} \\ \mathrm{THD}_{u,i}(\mathbf{X}) = \dfrac{\sqrt{\sum\limits_{h\in\Omega} U_{h,i}^2(\mathbf{X})}}{U_{1,i}} \times 100\% \leq \mathrm{THD}_{\max} \end{cases} \quad (i = 1, 2, 3) \tag{19}$$

where $U_{h,i}(\mathbf{X})$ is the rms value of the h-th harmonic voltage generated at the AC bus of node i under the current filter configuration $\mathbf{X}$; $U_{1,i}$ is the rated rms value of the fundamental voltage at this bus; and $\mathrm{HRU}_{\max}$ and $\mathrm{THD}_{\max}$ are the allowable upper limits of individual harmonic voltage distortion and total harmonic distortion specified by the national standard, as listed in Table 3.

The fitness values corresponding to each filter configuration are shown in Fig. 10.

5.2. Solution Method Based on DPSO

Since the number of double-tuned filter groups in service is an integer variable and multiple operating constraints must be satisfied simultaneously, the discrete particle swarm optimization (DPSO) algorithm is adopted to solve the model. The flowchart is illustrated in Fig. 9. DPSO has a simple structure, high search

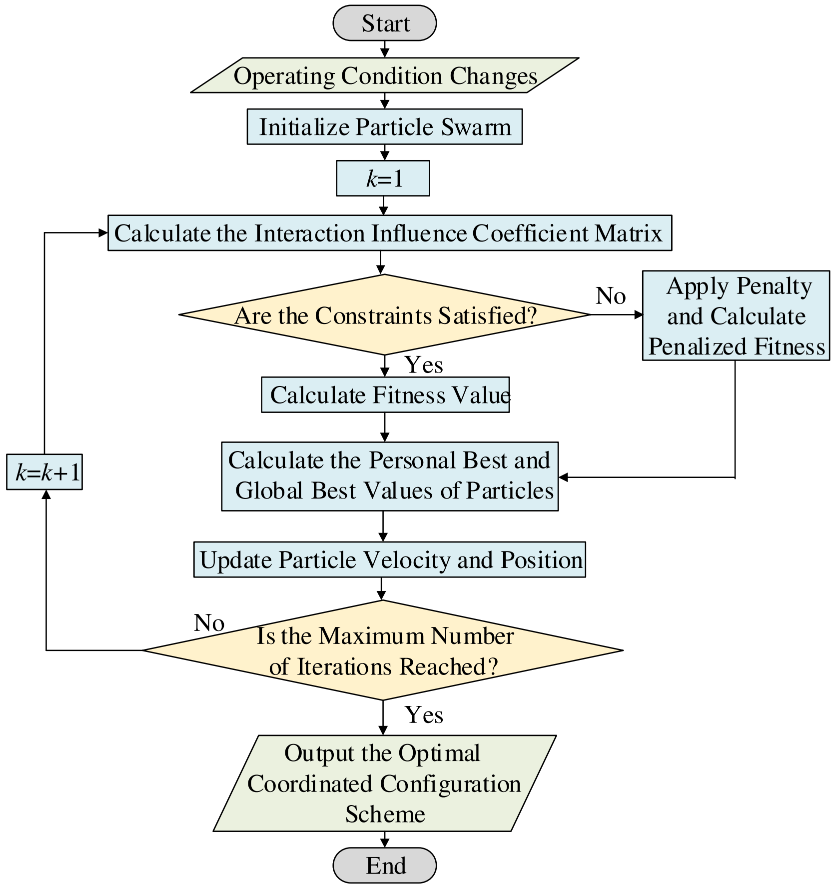

FIGURE 9. Flowchart of the DPSO algorithm.

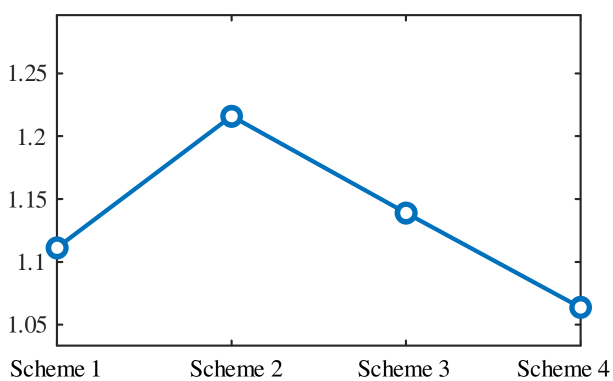

FIGURE 10. Fitness curves of the switching schemes.

efficiency, and good suitability for discrete combinatorial variables; therefore, it can search for a better switching scheme within a finite set of filter configurations.

In DPSO, each particle represents a filter switching combination. Let the position vector of the s-th particle at the t-th iteration be

$$\mathbf{X}_s^t = \left[X_{s,1}^t,\ X_{s,2}^t,\ \cdots,\ X_{s,D}^t\right] \tag{20}$$

where D is the dimension of the decision variables, and $X_{s,D}^t$ denotes the current value of the d-th decision variable. The corresponding velocity vector is expressed as

$$V_{s,d}^{t+1} = \omega V_{s,d}^t + c_1 r_1 \left(P_{s,d}^t - X_{s,d}^t\right) + c_2 r_2 \left(G_d^t - X_{s,d}^t\right) \tag{21}$$

where ω is the inertia weight; c_1 and c_2 are the cognitive and social learning factors, respectively; r_1 and r_2 are random numbers in the interval $[0, 1]$; $P_{s,d}^t$ is the historical best position of the particle itself; and G_d^t is the global best position of the swarm.

The decision variables are discrete integers, and the particle position must be updated together with the boundary correction after the velocity is updated to ensure that the integer condition is satisfied:

$$X_{s,d}^{t+1} = \text{round}\left(X_{s,d}^t + V_{s,d}^{t+1}\right) \tag{22}$$

If the updated particle position exceeds the allowable range, it is projected onto the corresponding boundary. The constraint repair is then performed on the particle position. If a particle violates the minimum or maximum number-of-groups constraint, the reactive power compensation constraint, or the minimum filter-configuration constraint, it is adjusted according to preset repair rules so that particles evaluated for fitness remain as close as possible to the feasible region.

To evaluate the suppression effect of different filter combinations on system harmonic interactions, the 11th and 13th characteristic harmonics were selected as the primary optimization targets. The set of characteristic harmonics Ω and the objective function for minimizing the overall system harmonic interaction are defined as follows:

$$\Omega = \{11, 13\} \tag{23}$$

TABLE 4. Optimized filter configuration schemes.

Scheme	Configuration of the first link		Configuration of the second link	
	DT11/24	DT13/36	DT11/24	DT13/36
Scheme 1	2	2	4	2
Scheme 2	3	1	4	2
Scheme 3	1	3	3	3
Scheme 4	2	2	3	3

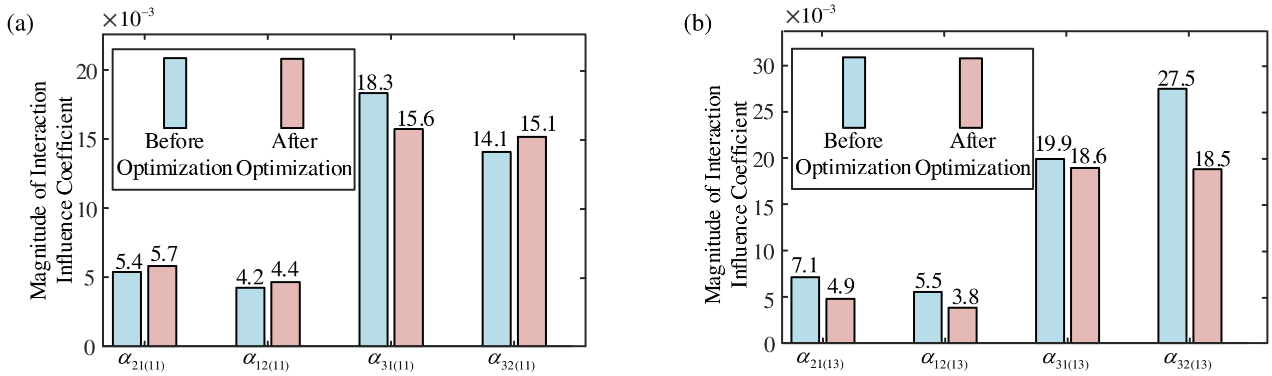

FIGURE 11. Changes in harmonic interaction influence coefficient magnitudes before and after filter optimization. (a) 11th harmonic and (b) 13th harmonic.

$$\min F(\mathbf{X}) = \sum_{h\in\Omega} \left(\begin{array}{c} \sum\limits_{i\in\{1,2\}} |\alpha_{ii}(h,\mathbf{X})| \\ + \sum\limits_{\substack{i,j\in\{1,2\} \\ i\neq j}} |\alpha_{ij}(h,\mathbf{X})| \\ + \sum\limits_{k\in\{1,2\}} |\alpha_{3k}(h,\mathbf{X})| \end{array} \right) \tag{24}$$

For each feasible particle, the harmonic current interaction influence coefficient matrix, the AC-bus harmonic currents in each branch, and the bus-voltage total harmonic distortion are first calculated according to each feasible particle's filter configuration vector $\mathbf{X}$, and all constraints are checked. For particles that violate the constraints, an exterior penalty function is introduced as follows:

$$F_{\text{pen}}(\mathbf{X}) = F(\mathbf{X}) + \gamma P(\mathbf{X}) \tag{25}$$

where γ is the penalty factor, and $P(\mathbf{X})$ is the constraint-violation function. For constraint-violating particles, a large penalty is imposed to reduce the probability of their selection as the optimal solution.

5.3. Case Study

The first conventional DC link was initially operated at 50% of the rated DC transmission power with eight double-tuned filter banks in service. The second conventional DC link operates at 40% of the rated DC transmission power, with six double-tuned filter groups in service. When the first conventional DC link is disturbed and its DC transmission power is reduced to 25%, the numbers of DT11/24 and DT13/36 filter groups in service must be adjusted to avoid reactive power overcompensation. Under these operating conditions, DPSO was used to optimize the double-tuned filter configurations of the two conventional HVDC converter stations. Infeasible schemes are screened out according to equipment configuration, minimum filtering, reactive power balance, and power-quality constraints; the candidate configuration schemes listed in Table 4 are thus obtained.

As shown in Fig. 10, the fitness values of the schemes differ significantly, indicating that the number of double-tuned filter groups directly affects the overall harmonic interaction level of the HMIDC system. Scheme 4 has the lowest fitness value, demonstrating that it achieves the best harmonic interaction suppression while satisfying all the operating constraints. Compared with the other schemes, Scheme 4 does not only reduce the number of filter groups in one link. Instead, it forms a more rational combination of filter groups between the two conventional DC links, thereby meeting the requirements of reactive power compensation, power quality, and harmonic interaction suppression simultaneously.

Figure 11 depicts alterations in the magnitudes of the harmonic current interaction influence coefficients among different DC links before and after optimization of the filter switching strategy. After conducting global optimization using DPSO, the interaction influence coefficients between the two conventional DC links at the 11th harmonic experience a slight increase. This indicates that, subject to reactive power compensation and minimum filtering requirement constraints, the optimization process does not minimize every interaction channel independently. Overall, the optimized scheme effectively mitigates the influence of the harmonic interaction of conventional HVDC links on the MMC-HVDC link. In particular, at the 13th harmonic, the interaction strength from the second conventional HVDC link to the MMC-HVDC link is reduced by approximately 32%. This result indicates that the proposed method is capable of reducing the harmonic interaction level of the HMIDC system from the overall system perspective while ensuring compliance with engineering operation constraints.

6. CONCLUSION

To tackle the challenge of quantifying the impact of AC filter switching on cross-station harmonic interactions in HMIDC systems, as well as the tendency of conventional filter configuration methods to emphasize local mitigation, this study establishes a filter configuration method oriented toward suppressing overall system harmonic interactions. The main conclusions are as follows:

The comprehensive evaluation index constructed using harmonic current interaction influence coefficients can simultaneously represent the local harmonic effect of each conventional DC link, the interaction between conventional DC links, and the harmonic influence of conventional DC links on the MMC-HVDC link. The normalized sensitivity analysis further shows that the AC filter parameters have a more significant influence on the comprehensive harmonic interaction index at the 11th and 13th characteristic harmonics. This indicates that variations in the AC filter impedance are important factors affecting the harmonic interaction strength of HMIDC systems. Therefore, coordinated AC filter switching provides a directly adjustable means of regulating harmonic current redistribution in HMIDC systems.

The influence of AC filter switching on harmonic interactions exhibits clear system coupling characteristics. After filters are switched out, the ability of the corresponding link to absorb characteristic harmonics decreases, and the harmonic current flowing into the AC system increases. Meanwhile, switching out the filters changes both the nodal impedance matrix and the current-distribution relationships among the DC links, and the harmonic currents in other DC links are also affected. Hence, in an HMIDC system, the AC filter configuration should not be determined only according to the reactive power demand or local harmonic level of a single converter station. The influence of this on the harmonic interaction strength of other links should also be considered.

The optimization model established with the numbers of double-tuned filter groups in service as discrete variables can coordinate the filter combinations of the two conventional HVDC converter stations under equipment configuration, minimum filtering requirements, reactive power compensation, and power-quality constraints. The case study results show that the optimized configuration reduces the overall system harmonic interaction level. In particular, at the 13th harmonic, the interaction strength from the second conventional HVDC link to the MMC-HVDC link decreases by approximately 32%. This indicates that the proposed method can improve the harmonic interaction characteristics of HMIDC systems while satisfying engineering operation constraints and can provide a reference for formulating AC filter switching strategies in hybrid multi-infeed DC systems.

ACKNOWLEDGMENT

This research was supported by the Science and Technology Project of Guangdong Power Grid Co., Ltd., under Grant No. GDKJXM20240406.

REFERENCES

[1] Rao, H., C. Hong, B. Zhou, D. Huang, S. Xu, W. Yao, *et al.*, "Study on improvement of VSC-HVDC at inverter side of wudongde multi-terminal UHVDC for the problem of centralized multi-infeed HVDC," *Southern Power System Technology*, Vol. 11, No. 3, 1–5, 2017.

[2] Dong, Z., G. Wang, Z. Xu, J. Li, and H. Ding, "Operation characteristic analysis method of Baihetan-Jiangsu hybrid cascaded UHVDC system," *Electric Power Automation Equipment*, Vol. 42, No. 6, 118–125, 2022.

[3] Hu, L. and R. Yacamini, "Harmonic transfer through converters and HVDC links," *IEEE Transactions on Power Electronics*, Vol. 7, No. 3, 514–525, 1992.

[4] Huang, H., J. Ma, S. Wang, Y. Dong, N. Jiao, and T. Liu, "Accurate analysis of harmonic transmission of line commutated converter considering firing angle fluctuation," *IEEE Access*, Vol. 8, 205 206–205 215, 2020.

[5] Wang, L., X. Zhang, T. Wang, and Z. Wang, "Harmonic characteristics of LCC-HVDC under unbalanced conditions," in *2023 IEEE International Symposium on Circuits and Systems (ISCAS)*, 1–5, Monterey, CA, USA, May 2023.

[6] Wang, S. L., Y. Xie, Y. Zhao, *et al.*, "Impedance modeling of 12-pulse converter station based on harmonic state space theory," *Southern Power System Technology*, Vol. 18, No. 6, 1–9, 2024.

[7] Zhou, P., T. Q. Liu, S. L. Wang, J. Ma, and H. Zhang, "Small signal modeling of LCC-HVDC station with consideration of harmonic coupling characteristics," *Power System Technology*, Vol. 45, No. 1, 153–161, 2021.

[8] Li, Q., Q. Zhou, D. Zhang, *et al.*, "A harmonic impedance scanning method of HVDC based on a test signal method," *Power System Protection and Control*, Vol. 49, No. 14, 168–175, 2021.

[9] Wang, G., Z.-K. Li, H.-F. Li, X.-L. Li, and C. Fu, "Calculation method of harmonic equivalent impedances of HVDC converter," *Proceedings of the CSEE*, Vol. 30, No. 19, 64–68, 2010.

[10] Riedel, P., "Harmonic voltage and current transfer, and AC-and DC-side impedances of HVDC converters," *IEEE Transactions on Power Delivery*, Vol. 20, No. 3, 2095–2099, 2005.

[11] Nian, H., L. Chen, Y. Xu, H. Huang, and J. Ma, "Sequences domain impedance modeling of three-phase grid-connected converter using harmonic transfer matrices," *IEEE Transactions on Energy Conversion*, Vol. 33, No. 2, 627–638, 2018.

[12] Sun, J. and H. Liu, "Sequence impedance modeling of modular multilevel converters," *IEEE Journal of Emerging and Selected Topics in Power Electronics*, Vol. 5, No. 4, 1427–1443, 2017.

[13] Chen, Y., L. Xu, A. Egea-Àlvarez, B. Marshall, M. H. Rahman, and A. D. Oluwole, "Mmc impedance modeling and interaction of converters in close proximity," *IEEE Journal of Emerging and Selected Topics in Power Electronics*, Vol. 9, No. 6, 7223–7236, 2021.

[14] Chen, X., A. M. Gole, and M. Han, "Analysis of mixed inverter/rectifier multi-infeed HVDC systems," *IEEE Transactions on Power Delivery*, Vol. 27, No. 3, 1565–1573, 2012.

[15] Xiao, H. and Y. Li, "Multi-Infeed voltage interaction factor: A unified measure of inter-inverter interactions in hybrid multi-infeed HVDC systems," *IEEE Transactions on Power Delivery*, Vol. 35, No. 4, 2040–2048, 2020.

[16] Yin, H., X. Zhou, Y. Liu, H. Xia, L. Hong, R. Zhu, and L. Deng, "Interaction mechanism analysis and additional damping control for hybrid multi-infeed HVDC system," *IEEE Transactions on Power Delivery*, Vol. 37, No. 5, 3904–3916, 2022.

[17] Liu, T., J. Wen, G. Qiao, Q. Fu, and S. Zhou, "Study on harmonic effects of multi-infeed HVDC systems," *Advanced Technology of Electrical Engineering and Energy*, Vol. 35, No. 1, 42–47, 2016.

[18] Mao, X., W. He, and Z. Zhou, "Comparison of calculation methods for multi-infeed interaction factors," *Advanced Technology of Electrical Engineering and Energy*, Vol. 40, No. 5, 57–63, 2021.

[19] Li, Z., "Analysis of harmonic interaction in hybrid multi-infeed HVDC system," South China University of Technology, Guangzhou, China, 2020.

[20] Wen, J., W. Meng, W. Yin, *et al.*, "Optimizing design of AC filters of ±800 kV UHVDC transmission projects," *High Voltage Engineering*, Vol. 36, No. 4, 912–917, 2010.

[21] Kahar, N. H. A., A. F. Zobaa, R. A. Turky, A. M. Zobaa, S. H. E. A. Aleem, and B. Ismail, "Comparative analysis of optimal damped and undamped passive filters using MIDACO-solver," *Ain Shams Engineering Journal*, Vol. 14, No. 8, 102056, 2023.

[22] Wang, J., M. Chen, S. Yu, and X. Zhang, "Review of modeling and analysis of parasitics in power electronic converters," *Chinese Journal of Electrical Engineering*, Vol. 11, No. 1, 151–173, 2025.